Support Information

Single-atom supported on MXenes for alkaline hydrogen evolution reaction: species, coordination environment, and action mechanism

Zijun Sun [1,2], Rui Li [1,2,*], Qing Xi [1,2], Fangxia Xie [1,2], Xuan Jian [3], Xiaoming Gao [3], Houfen Li [1], Zhuobin Yu [1], Jianxin Liu [1,2], Xiaochao Zhang [2], Yawen Wang [2], Yunfang Wang [2], Xiuping Yue [1,2,*], Caimei Fan [1,2]

[1] *College of Environmental Science and Engineering, Taiyuan University of Technology, Taiyuan 030024, P. R. China*

[2] *College of Chemical Engineering and Technology, Taiyuan University of Technology, Taiyuan 030024, P. R. China*

[3] *College of Chemistry and Chemical Engineering, Shaanxi Key Laboratory of Chemical Reaction Engineering, Yan'an University, Yan'an 716000, P. R. China*

*Co-corresponding author.

Tel.: +86 13233699182; +86 13068076599; fax: +86 351 6018554.

E-mail address: lirui13233699182@163.com (Li R); yuexiuping@tyut.edu.cn (Yue XP).

Table S1 Mo-based MXenes alkaline HER performance descriptor.

Mo-based MXenes	ΔG_{*H2O} (eV)	$\Delta G_{*H\text{-}OH}$ (eV)	ΔG_{*H} (eV)	ΔG_{*OH} (eV)
Mo_2CO_2	0.486	2.204	-0.430	-2.291
$Mo_2TiC_2O_2$	0.348	2.767	-0.373	-2.658
$Mo_2Ti_2C_2O_2$	0.379	2.775	-0.229	-2.553

Table S2 Ground state magnetic moment of TM single atom in TM-$Mo_2Ti_2C_3O_2$ systems (in Bohr magnetons, μB).

TM-$Mo_2Ti_2C_3O_2$	Magnetic moment (μB)	TM-$Mo_2Ti_2C_3O_2$	Magnetic moment (μB)
Fe_A-$Mo_2Ti_2C_3O_2$	0	Co_A-$Mo_2Ti_2C_3O_2$	0
Fe_B-$Mo_2Ti_2C_3O_2$	3.277	Co_B-$Mo_2Ti_2C_3O_2$	-0.004
Fe_S-$Mo_2Ti_2C_3O_2$	2.952	Co_S-$Mo_2Ti_2C_3O_2$	0.005
Ni_A-$Mo_2Ti_2C_3O_2$	0	Ru_A-$Mo_2Ti_2C_3O_2$	0
Ni_B-$Mo_2Ti_2C_3O_2$	0	Ru_B-$Mo_2Ti_2C_3O_2$	2.574
Ni_S-$Mo_2Ti_2C_3O_2$	0	Ru_S-$Mo_2Ti_2C_3O_2$	1.970
Rh_A-$Mo_2Ti_2C_3O_2$	0	Pd_A-$Mo_2Ti_2C_3O_2$	0
Rh_B-$Mo_2Ti_2C_3O_2$	1.645	Pd_B-$Mo_2Ti_2C_3O_2$	0.291
Rh_S-$Mo_2Ti_2C_3O_2$	0.668	Pd_S-$Mo_2Ti_2C_3O_2$	0
Os_A-$Mo_2Ti_2C_3O_2$	0	Ir_A-$Mo_2Ti_2C_3O_2$	0
Os_B-$Mo_2Ti_2C_3O_2$	2.598	Ir_B-$Mo_2Ti_2C_3O_2$	1.582
Os_S-$Mo_2Ti_2C_3O_2$	1.964	Ir_S-$Mo_2Ti_2C_3O_2$	0.276
Pt_A-$Mo_2Ti_2C_3O_2$	0		
Pt_B-$Mo_2Ti_2C_3O_2$	0.716		
Pt_S-$Mo_2Ti_2C_3O_2$	0		

Table S3 Ru-$Mo_2Ti_2C_3O_2$ alkaline HER performance descriptor.

TM-$Mo_2Ti_2C_3O_2$	ΔG_{*H2O} (eV)	$\Delta G_{*H\text{-}OH}$ (eV)	ΔG_{*H} (eV)	ΔG_{*OH} (eV)	i_0 (Acm^{-2})
Fe_A-$Mo_2Ti_2C_2O_2$	0.3676	1.0737	-0.2111	-1.5668	-3.5697
Fe_B-$Mo_2Ti_2C_2O_2$	0.5264	0.4592	1.7797	0.0239	-30.0906
Fe_S-$Mo_2Ti_2C_2O_2$	0.8802	0.3348	0.1161	1.2328	-1.9635
Co_A-$Mo_2Ti_2C_2O_2$	0.2451	0.8530	-0.8313	-1.1797	-14.0561
Co_B-$Mo_2Ti_2C_2O_2$	-0.7968	1.7020	1.0859	0.0831	-18.3612
Cos-$Mo_2Ti_2C_2O_2$	-0.5491	0.6067	-0.0792	0.6505	-1.3397
Ni_A-$Mo_2Ti_2C_2O_2$	0.2855	1.1009	-0.4513	-1.5411	-7.6310
Ni_B-$Mo_2Ti_2C_2O_2$	-0.5653	1.0312	0.1652	0.4244	-2.7934
Ni_S-$Mo_2Ti_2C_2O_2$	-0.7383	1.1234	0.0226	0.0629	-0.3816
Ru_A-$Mo_2Ti_2C_2O_2$	0.3831	1.8965	-0.1457	-2.0335	-2.4635
Ru_B-$Mo_2Ti_2C_2O_2$	-0.8891	0.0125	0.1817	1.3783	-3.0717
Ru_S-$Mo_2Ti_2C_2O_2$	-0.7781	0.2919	-0.0414	1.1997	-0.7008
Rh_A-$Mo_2Ti_2C_2O_2$	0.3876	0.5782	-0.8811	-1.0948	-14.8969
Rh_B-$Mo_2Ti_2C_2O_2$	-0.7140	0.3325	0.2363	0.9188	-3.9948
Rh_S-$Mo_2Ti_2C_2O_2$	-0.4915	0.9021	-0.3595	0.5226	-6.0783
Pd_A-$Mo_2Ti_2C_2O_2$	0.2837	1.1331	-0.4799	-1.5222	-8.1137
Pd_B-$Mo_2Ti_2C_2O_2$	-0.4037	1.0637	-0.0526	0.1204	-0.8891
Pd_S-$Mo_2Ti_2C_2O_2$	-0.3527	1.6609	0.0134	-0.7866	-0.2272
Os_A-$Mo_2Ti_2C_2O_2$	0.3897	2.5556	-0.0964	-2.3256	-1.6295
Os_B-$Mo_2Ti_2C_2O_2$	-1.6317	-0.8483	-1.0337	2.2875	-17.4784
Os_S-$Mo_2Ti_2C_2O_2$	-0.9359	0.0786	0.0254	1.4819	-0.4289
Ir_A-$Mo_2Ti_2C_2O_2$	0.3909	1.0657	-0.0394	-1.6411	-0.6655
Ir_B-$Mo_2Ti_2C_2O_2$	-0.7937	-0.6342	-0.1074	1.5538	-1.8165
Ir_S-$Mo_2Ti_2C_2O_2$	-0.4723	0.3737	-0.3970	0.8041	-6.7125
Pt_A-$Mo_2Ti_2C_2O_2$	0.2860	1.1875	-0.4691	-1.5434	-7.9308
Pt_B-$Mo_2Ti_2C_2O_2$	-1.1703	0.0332	-0.3101	0.9464	-5.2426
Pt_S-$Mo_2Ti_2C_2O_2$	-0.4051	0.9475	-0.0356	-0.2535	-0.6022

Table S4 Calculated standard potentials for reactions given by Equation (1) to (4), standard conditions, 298.15 K, pH = 0.

	z	$E^0(M^{z+}/Mo_2Ti_2C_3O_2)$/V	E^0(TM-$Mo_2Ti_2C_3O_2$/H-TM-$Mo_2Ti_2C_3O_2$)/V	E^0(OH-TM-$Mo_2Ti_2C_3O_2$/TM-$Mo_2Ti_2C_3O_2$)/V	E^0(H-TM-$Mo_2Ti_2C_3O_2$/TM-$Mo_2Ti_2C_3O_2$)/V
Fe_A	3	2.836			
Fe_B	3	1.047	-1.640	0.282	0.413
Fe_S	3	0.870	0.154	-0.985	0.210
Co_A	2	4.602			
Co_B	2	2.126	-0.464	0.223	1.014
Co_S	2	2.357	-1.153	-0.403	0.981
Ni_A	2	3.740			
Ni_B	2	1.382	0.900	-0.118	0.731
Ni_S	2	2.097	-1.321	0.184	1.259
Ru_A	3	3.714			
Ru_B	3	0.914	-0.028	-1.072	-0.278
Ru_S	3	1.515	-0.897	-0.952	0.643
Rh_A	3	2.827			
Rh_B	3	0.783	-0.332	-0.613	0.471
Rh_S	3	1.517	-0.818	-0.276	0.629
Pd_A	2	2.956			
Pd_B	2	0.781	-0.198	0.185	1.133

Pd_S	2	1.973	-1.646	1.033	1.824

	z	$E^0(M^{z+}/Mo_2Ti_2C_3O_2)$/V	E^0(TM-$Mo_2Ti_2C_3O_2$/H-TM-$Mo_2Ti_2C_3O_2$)/V	E^0(OH-TM-$Mo_2Ti_2C_3O_2$/TM-$Mo_2Ti_2C_3O_2$)/V	E^0(H-TM-$Mo_2Ti_2C_3O_2$/TM-$Mo_2Ti_2C_3O_2$)/V
Os_A	4	3.174			
Os_B	4	0.458	0.389	-1.981	-1.005
Os_S	4	1.208	-0.384	-1.234	0.257
Ir_A	3	3.342			
Ir_B	3	0.663	0.772	-1.247	-0.150
Ir_S	3	1.731	-0.370	-0.557	0.687
Pt_A	2	3.811			
Pt_B	2	0.782	0.523	-0.640	0.480
Pt_S	2	2.692	-1.032	0.500	1.417

We consider the following electrochemical reaction processes on the surface of MXenes-supported metal SACs:

$$TM^{z+}+ze^-+Mo_2Ti_2C_3O_2 \rightarrow TM\text{-}Mo_2Ti_2C_3O_2 \quad (1)$$

$$TM\text{-}Mo_2Ti_2C_3O_2+H^++e^- \rightarrow H\text{-}TM\text{-}Mo_2Ti_2C_3O_2 \quad (2)$$

$$OH\text{-}TM\text{-}Mo_2Ti_2C_3O_2+H^++e^- \rightarrow TM\text{-}Mo_2Ti_2C_3O_2+H_2O \quad (3)$$

$$O\text{-}TM\text{-}Mo_2Ti_2C_3O_2+2H^++2e^- \rightarrow TM\text{-}Mo_2Ti_2C_3O_2+H_2O \quad (4)$$

Since the TM single atom in TM_A-$Mo_2Ti_2C_3O_2$ is not modified on the surface of $Mo_2Ti_2C_3O_2$, we only calculated the pourbaix diagram of the TM^{z+} confinement process (Equation (1)) in this case.

The pourbaix diagrams of TM_A-$Mo_2Ti_2C_3O_2$, TM_B-$Mo_2Ti_2C_3O_2$, and TM_S-$Mo_2Ti_2C_3O_2$ at 298.15K are shown in Fig. S1, S2, and S3, respectively. It can be seen from Fig. S1 that the potential of metal dissolution in TM_A-$Mo_2Ti_2C_3O_2$ is at least 2.8 eV (see Table S4), which proves that TM single atom has high stability after anchoring to Mo defects and will not be easily dissolved from the catalyst.

In TM_B-$Mo_2Ti_2C_3O_2$ and TM_S-$Mo_2Ti_2C_3O_2$ (see Fig. S2 and S3), transition metal single atom is difficult to dissolve from the catalyst in all cases, which proves that the single atom site in the studied single atom catalyst has high stability under operating conditions. At E = 0 eV, Ni_B-$Mo_2Ti_2C_3O_2$ exhibits hydrogenophilic properties in all pH ranges, indicating the surface of the catalyst is easily covered by H. While the surface of Os_B, Ir_B, Pt_B, Fe_S, Ru_B, Rh_B, Os_B, Co_S, Ru_S, Os_S, Ir_S-$Mo_2Ti_2C_3O_2$ will be covered by H or OH, depending on the pH value. The TM single atom in the remaining TM-$Mo_2Ti_2C_3O_2$ (such as Fe_B, Co_B, Pd_B, Ni_S, Pd_S, and Pt_S-$Mo_2Ti_2C_3O_2$) can be stably exposed under certain pH and voltage conditions.

For Ru_S-$Mo_2Ti_2C_3O_2$, which we finally screened out as an excellent hydrogen evolution catalyst, the adsorption of OH on the Ru site is stable at pH = 14, and the adsorption of H on the Ru site is the most stable at -1.78 V. There is a strong interaction between OH and Ru, which is consistent with the conclusion in Fig. 5a. This phenomenon indicates that the OH desorption process in the alkaline hydrogen evolution reaction is the potential determining step.

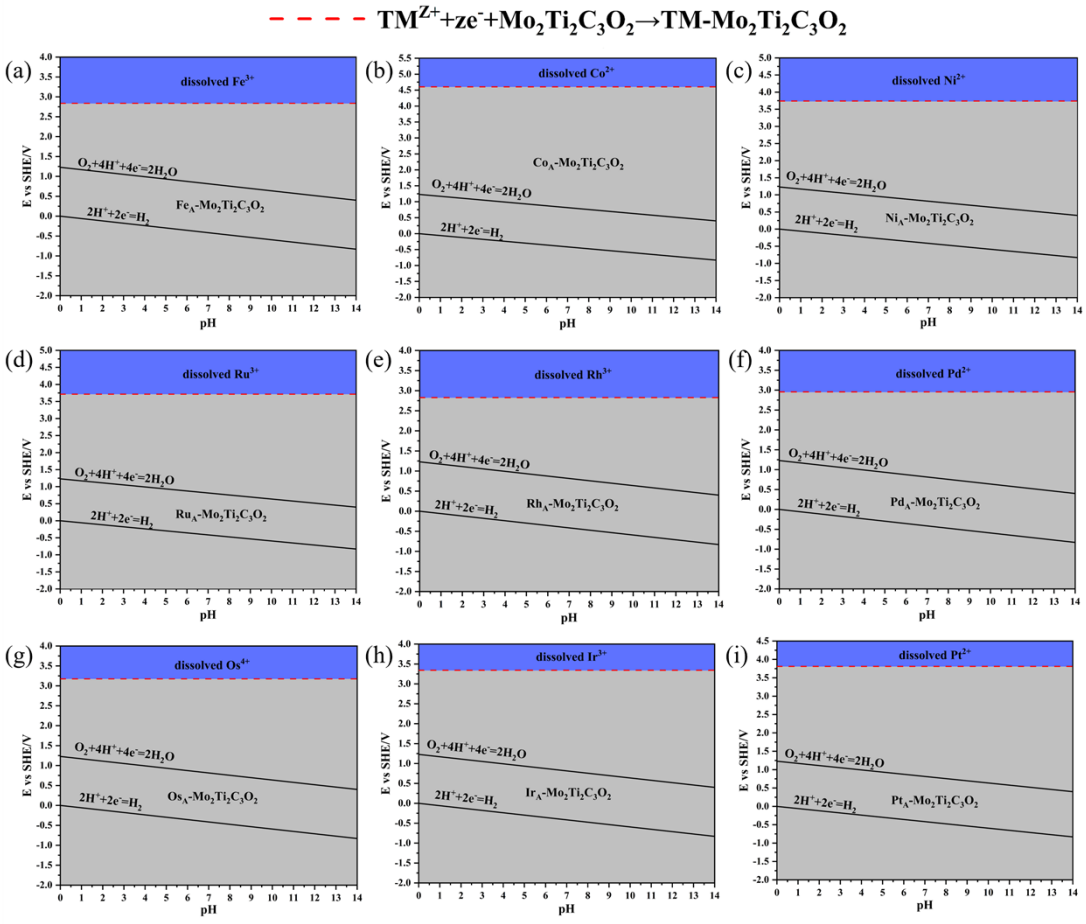

Fig. S1 Surface Pourbaix plots for TM_A-$Mo_2Ti_2C_3O_2$. Thick black lines indicate the theoretical water stability region.

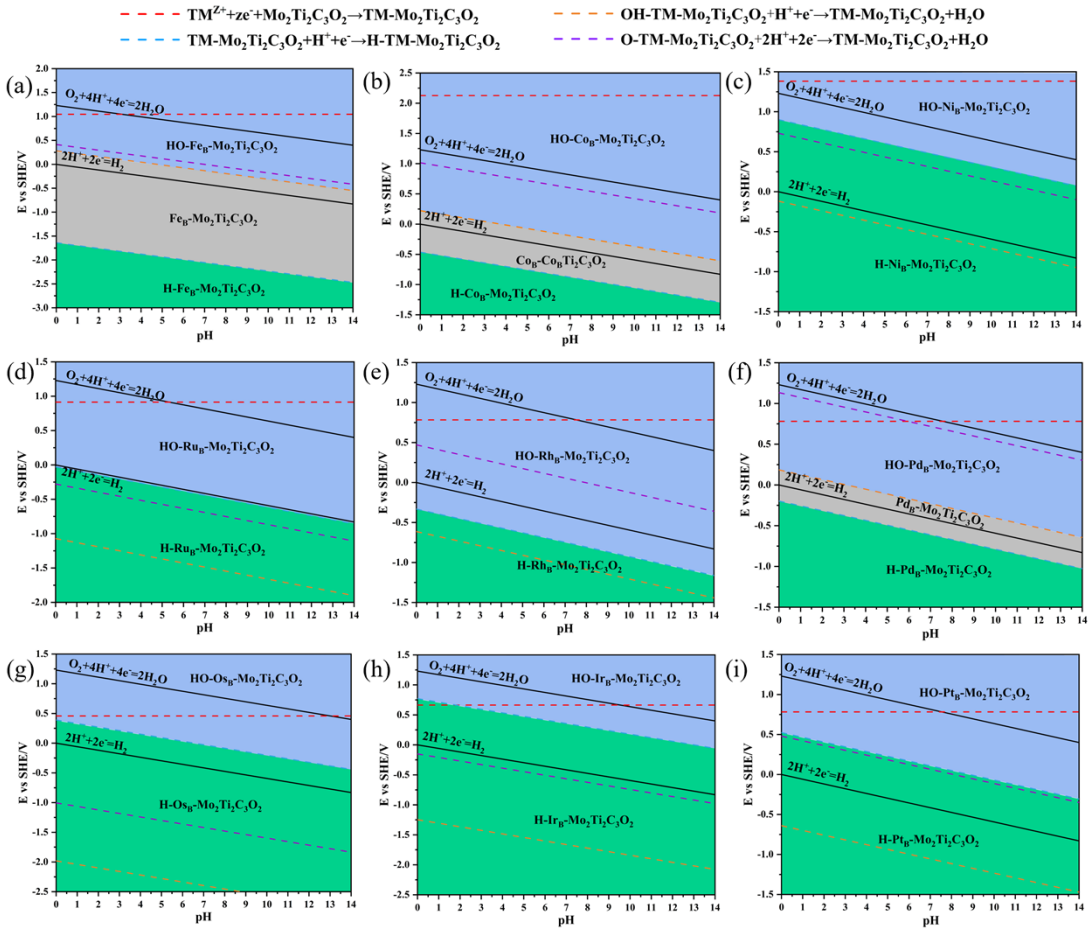

Fig. S2 Surface Pourbaix plots for TM_B-$Mo_2Ti_2C_3O_2$. Thick black lines indicate the theoretical water stability region.

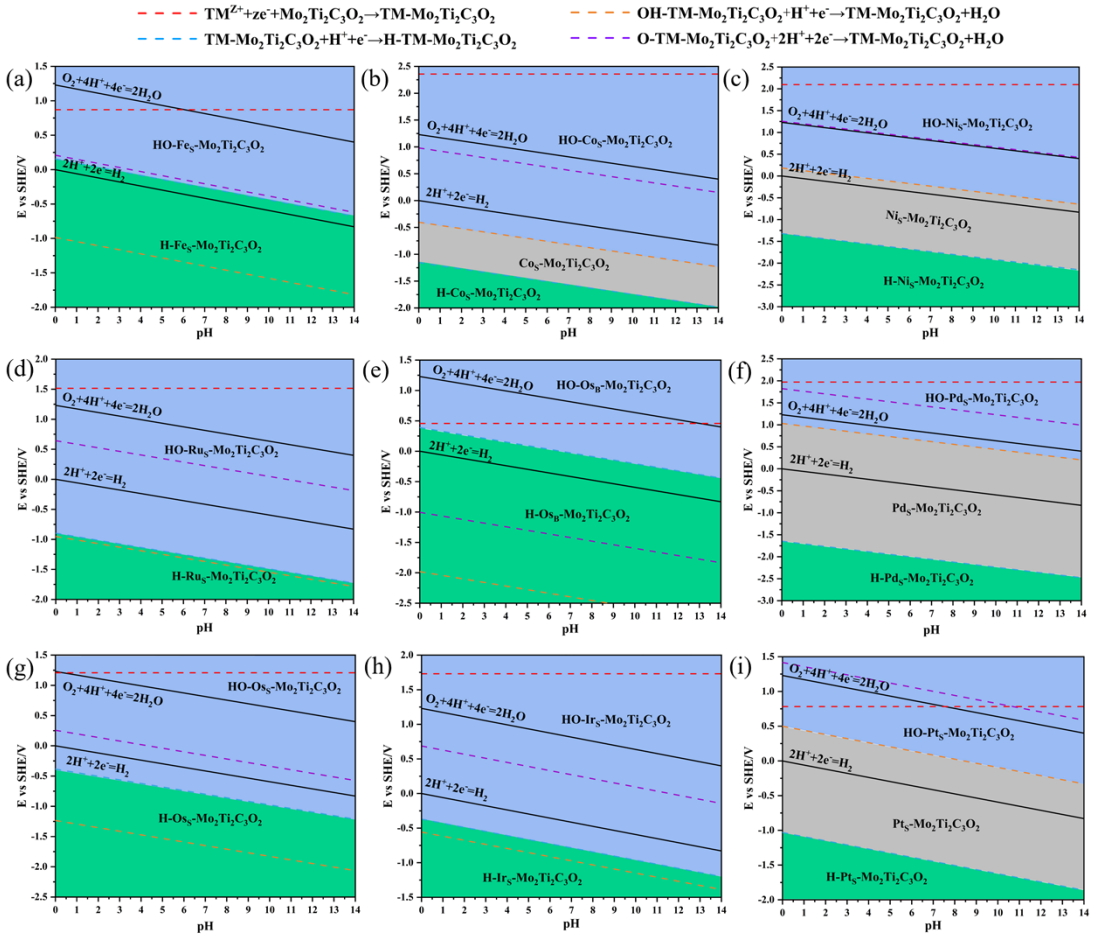

Fig. S3 Surface Pourbaix plots for TM_S-$Mo_2Ti_2C_3O_2$. Thick black lines indicate the theoretical water stability region.

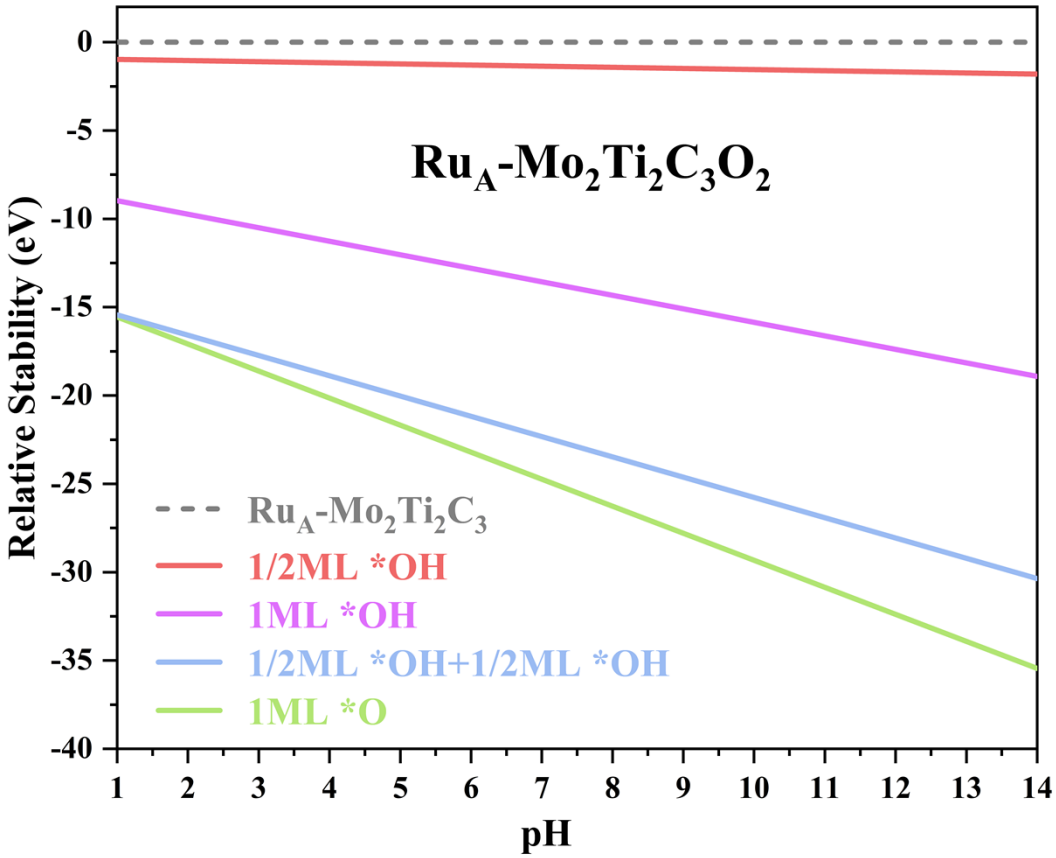

Fig. S4 The relative stability of *O and *OH was terminated on Ru_A-$Mo_2Ti_2C_3$ at U_{SHE} = 0 V.

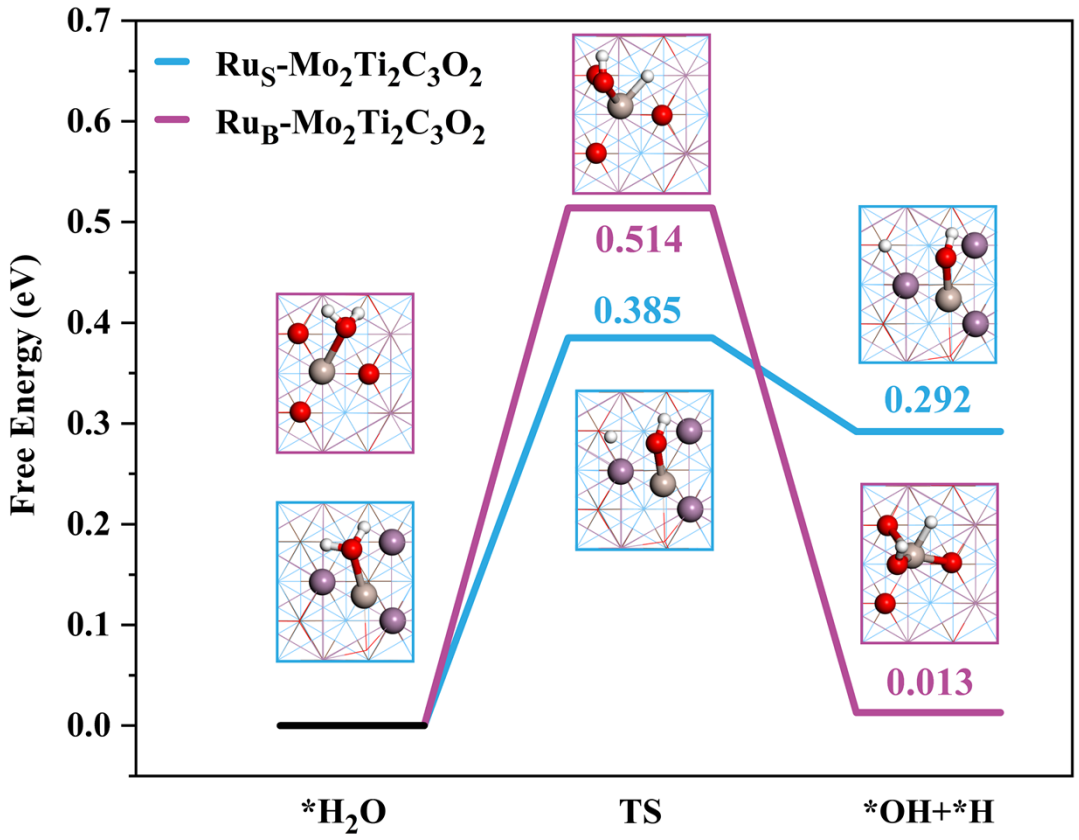

Fig. S5 Reaction energy diagram of water dissociation on Ru_S-$Mo_2Ti_2C_2O_2$ and Ru_B-$Mo_2Ti_2C_2O_2$.

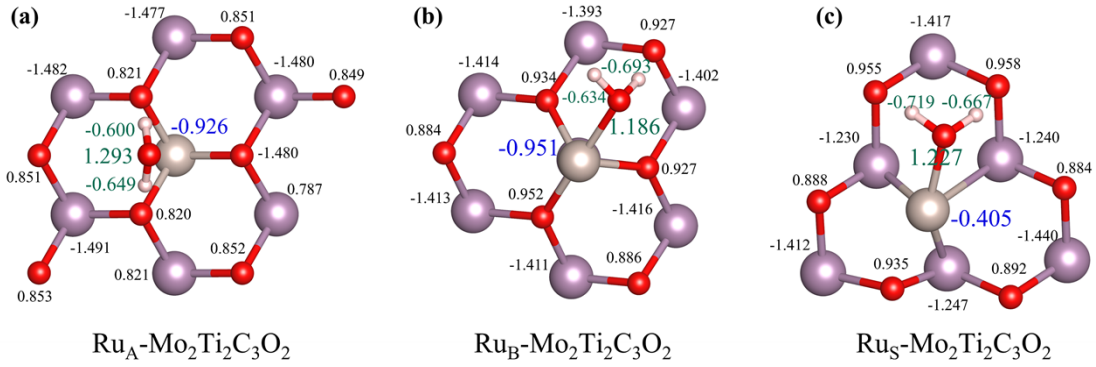

Ru_A-$Mo_2Ti_2C_3O_2$ Ru_B-$Mo_2Ti_2C_3O_2$ Ru_S-$Mo_2Ti_2C_3O_2$

Fig. S6 Bader charge analysis of H_2O adsorption in Ru-$Mo_2Ti_2C_2O_2$

Through the comparison between Fig. 4d-f and Fig. S1a-c, it can be found that the Ru atom on Ru_A-$Mo_2Ti_2C_2O_2$ obtains electrons after adsorbing H_2O molecules, indicating that this Ru atom is an electron acceptor. Similarly, the single Ru atom in Ru_S-$Mo_2Ti_2C_2O_2$ and Ru_B-$Mo_2Ti_2C_2O_2$ are electron donors, which is the reason for the effective activation of H_2O.